Comparison of the Fracture and Failure Behavior of Injection-Molded α- and β-Polypropylene in High-Speed Three-Point Bending Tests

J. KARGER-KOCSIS,[1] J. VARGA,[2] G. W. EHRENSTEIN[3]

[1]Institut für Verbundwerkstoffe GmbH, Universität Kaiserslautern, Pf. 3049, D-67653 Kaiserslautern, Germany

[2]Department of Plastics and Rubber Technology, Technical University of Budapest, H-1521 Budapest, Hungary

[3]Lehrstuhl für Kunststofftechnik, Universität Erlangen-Nürnberg, D-91058 Erlangen, Germany

Received 6 May 1996; accepted 6 September 1996

ABSTRACT: The fracture and failure mode of α- and β-isotactic polypropylene (α-iPP and β-iPP, respectively) were studied in high speed (1 m/s) three-point bending tests on notched bars cut from injection-molded dumbbell specimens and compared. The fracture response of the notched Charpy-type specimens at room temperature (RT) and -40°C, respectively, was described by terms of the linear elastic fracture mechanics (LEFM), namely fracture toughness (K_c) and fracture energy (G_c). K_c values of both iPP modifications were similar, while G_c values of the β-iPP were approximately twofold of the reference α-iPP irrespective of the test temperature. It was demonstrated that β-iPP failed in a ductile and brittle–microductile manner at RT and -40°C, respectively. By contrast, brittle fracture dominated in α-iPP at both testing temperatures. Based on the fracture surface appearance, it was supposed that β-to-α ($\beta\alpha$) transformation occurred in β-iPP. The superior fracture energy of β-iPP to α-iPP was attributed to a combined effect of the following terms: morphology, mechanical damping, and phase transformation. Results indicate that their relative contribution is a function of the test temperature. © 1997 John Wiley & Sons, Inc. J Appl Polym Sci **64:** 2057–2066, 1997

Key words: α-polypropylene; β-polypropylene; failure; fracture mechanics; injection molding; phase transformation toughening

INTRODUCTION

As reviewed recently,[1,2] the β-modification of isotactic polypropylene (β-iPP) can be produced in pure[3] or nearly pure[4] form by adding adequate nucleants and selecting proper thermal conditions for crystallization. β-iPP exhibits some peculiar thermal and mechanical properties. Padden and Keith reported that β-iPP recrystallizes into the α-modification ($\beta\alpha$-transition) during partial melting.[5] It was clarified later that this thermally induced $\beta\alpha$-transition is controlled by the thermal history of the β-crystalline phase.[1–3] Varga has shown that β-iPP samples undergo $\beta\alpha$-transition only if they were cooled below a critical temperature ($T \approx 100 \cdots 106$°C) prior to melting.[3] According to the observations of the group of Fujiwara,[6–8] Varga,[1,2] and Shi et al.,[9] this $\beta\alpha$-transformation can also be induced by mechanical loading. Based on differential scanning calorimetric (DSC) studies performed on the necked region of uniaxially loaded dumbbell specimens by Varga,[1] it was shown that this $\beta\alpha$-transition strongly depends on the strain under both cold

Correspondence to: J. Karger-Kocsis (karger@ivw.uni-kl.de).
 CCC 0021-8995/97/112057-10

and hot stretching conditions. Karger-Kocsis proposed recently that the phase transformation toughening (PTT) can work also in semicrystalline polymers and demonstrated the viability of his concept on an example of the $\beta\alpha$-transition in iPP.[10,11]

The present state of knowledge on the uniaxial tensile stress-induced $\beta\alpha$ transformation in iPP and on related change in the toughness can be summarized as follows:

1. The $\beta\alpha$-transformation is strain-dependent. With increasing strain the fractional $\beta\alpha$ conversion is increasing as well.[1,2,12] It should be noted here that the mechanism of this $\beta\alpha$-transition is not well understood yet.[6–8]
2. The $\beta\alpha$-transition depends also on the frequency of the mechanical test. With increasing test frequency or strain rate the conversion of the $\beta\alpha$-transformation is reduced. This was associated with an opposite change in the toughness, which increased considerably.[12]
3. The plastic deformation of β-iPP is associated with microvoiding, which is caused by a complex interaction of the morphology-controlled inherent ductility and volume contraction due to the $\beta\alpha$- or β-smectic transition.[13] Recall that the $\beta\alpha$-transition goes from a less toward a more dense crystalline form, so it is associated with contraction. The microvoided area, representing the plastic or damage zone in the loaded specimens, can well be observed by the characteristic stress-whitening (light scattering caused by the microvoids[11,12]).

There are several reports in the open literature claiming that toughness of β-iPP is superior to the related α-modification also when instead of uniaxial tensile deformation high-speed flexural loading is used.[14–18] These reports are based either on standard Izod,[14,15] Charpy (three-point-bending),[16,17] or Dynstat tests.[18] It is worth noting that Tjong et al. reported on a toughness increase of 27% (fracture energy determined on notched injection-molded Charpy bars at room temperature, RT).[16,17] This improvement can be estimated as $\approx$ 300% (surface-related impact energy from standard Izod test at RT—Fujiyama[15]), $\approx$ 47% (notch-length-related impact energy from standard Izod tests on injection molded specimens at RT—Jacoby et al.[14]), and $\approx$ 27% (fracture-surface-related impact energy from Dynstat test at -50°C—Varga[18]). Surprisingly, none of the cited authors claimed or demonstrated that the toughness increase in high-speed fracture would occur via PTT. Considering the static[10–12] and dynamic tensile results on β-iPP,[12] where the occurrence of the $\beta\alpha$-transition was evidenced, it is reasonable to assume that PTT works also in high-speed three-point bending impact.

It should be underlined here that the work of Tjong et al. is the first comparison of the fracture response of α- and β-iPP by using the concept of the linear elastic fracture mechanics (LEFM).[16,17] The fracture mechanical approach is the only correct way when the toughness comparison between various iPP modifications is tackled. Concepts of the fracture mechanics, in fact, yield an inherent material parameter which is independent of the testing configuration.

The aim of this study was to determine and compare the fracture mechanical response of α-iPP and β-iPP, derived from high-speed three-point bending by using notched Charpy bars. A further aim of this work was to collate the results with those of Tjong et al.[16,17] In order to do this, specimen preparation and testing conditions (especially impact speed) similar to those used by Tjong and colleagues were adopted. Special attention was paid to the detection of the supposed $\beta\alpha$-transformation. This aspect was triggered by our impression that the fractographic work published[15–17] can hardly explain the large toughness difference found between α- and β-iPP.

EXPERIMENTAL

β-iPP was produced by extrusion compounding of a general purpose extrusion molding iPP grade (Tipplen H 791F, MFI at 230°C and 21.2 N; load: 0.8 dg/min; supplier: Tisza Chemical Works Ltd., Hungary) with 0.1 wt % proprietary β-nucleant of modified γ-quinacridone type. From the pelletized β- and α-iPP (the latter was also passed through the extruder in order to set the same thermal prehistory), film-gated tensile bars (dumbbell specimen according to the ISO 3167 standard) were injection molded at the following conditions: melt temperature, 260°C; mold temperature, 100°C; injection speed, 20 mm/s. The presence of β-iPP and the overall crystallinity of the specimens were detected by differential scanning calorimetry (DSC 30 of Mettler) at 10°C/min heating rate. Accepting a melting enthalpy of 148

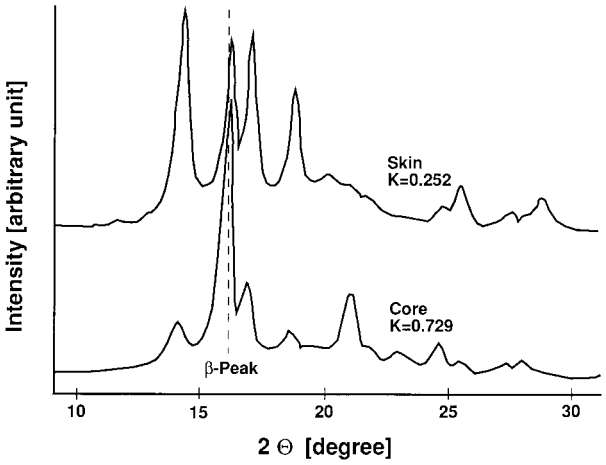

Figure 1 WAXS patterns representing the core and skin region of the injection-molded β-iPP dumbbell specimen.

J/g for the fully crystalline iPP,[19] the average crystallinity of both samples was 60–65%. Unfortunately, the relative β-content of the β-iPP could not be derived from DSC tests because of the superimposed thermally induced βα-recrystallization process (see above). Therefore, wide-angle X-ray scattering (WAXS) patterns were taken both from the core (after removing the molding-induced skin layers, see later) and skin layers of the tensile bars. WAXS was performed in a Phillips Micro Müller 111 device by using Ni-filtered CuK_α radiation. Figure 1 makes obvious that the β-content in the core is markedly higher than that in the skin. This is due to the fact that melt shearing in iPP is associated with the formation of α-row nuclei.[2,20] As a consequence in the skin, where shear stresses prevailed, the α-phase is enriched. Based on the WAXS patterns in Figure 1, the relative β-content was determined by the method of Turner-Jones et al.[21] This method yielded a K value of 0.25 and 0.73 for the skin and core layers, respectively.

The complex dynamic E-modulus (E^*) and mechanical loss factor ($tg\,\delta$) were monitored as a function of temperature (T) by a dynamic-mechanical thermoanalyzer (DMTA; Eplexor 150 N) of Gabo Qualimeter (Ahlden, Germany). DMTA spectra were taken in three-point bending under load-controlled sinusoidal excitation (mean static load: 10 N with a superimposed oscillating part ±5 N) at constant frequency (f = 10 Hz). Rectangular bars of 50 × 10 × 4 mm^3 (length × width × thickness) were cut from the gauge section of the dumbbells by means of a Cutvis device of Ceast (Turin, Italy). The specimen preparation technique of Tjong et al. was followed.[16,17]

Fracture toughness (critical stress intensity factor, K_c) and fracture energy (critical strain energy release rate, G_c) were determined in three-point bending (flexural) tests on razor blade notched specimens. The notch depth (a) was set in the range of a/W = 0.4 to 0.5 where W = width (see Fig. 2).

The notched Charpy bars were impacted by an instrumented impact pendulum of Ceast, equipped with an AFS MK3 data acquisition unit, at v = 1 m/s at room temperature (RT) and T = −40°C, respectively. Impacting of the specimens occurred under the following conditions: mass of the striker = 2.19 kg (yielding an impact energy of 1 J at v = 1 m/s), striker working range = 0.55 kN, testing time up to 8 ms (with data sampling of 4 μs interval). The related software allowed us to display the fracture process in different graphs from which the load (F) and energy (E) versus time (t), and F and E versus deflection (x) traces were preferentially used. From the fractograms recorded, the maximum load (F_{max}), the energy absorbed up to F_{max} (energy required for fracture initiation, E_{init}), and the full energy absorbed (E_{total}) were read or computed. For K_c (based on F_{max}) and G_c (based on E_{init}) determination, the recommendations of the ESIS TC-4 group were adopted (see also Fig. 2).[22] In respect to G_c, this approach agrees basically with that of Plati and Williams.[23] Fracture mechanical data included in this paper represent mean values of five to seven measurements carried out on specimens of similar a/W ratio. The fracture surface of the specimens was analyzed in a scanning electron microscope (SEM; Jeol JSM 5400) after gold coating.

RESULTS AND DISCUSSION

Effect of Temperature

Figure 3 displays characteristic (F,E)–t traces at T − 40°C for the α-iPP and β-iPP, respectively. Comparing the E–t traces in Figure 3(a) and Figure 3(b), and keeping in mind that the fracture response is directly comparable due to the same a/W ratio selected, the superior toughness of β-iPP to α-iPP becomes obvious. Moreover, the fractograms (F–t traces) indicate that β-iPP failed ductilely with considerable crack propagation [E_{prop}; see Fig. 3(b)].

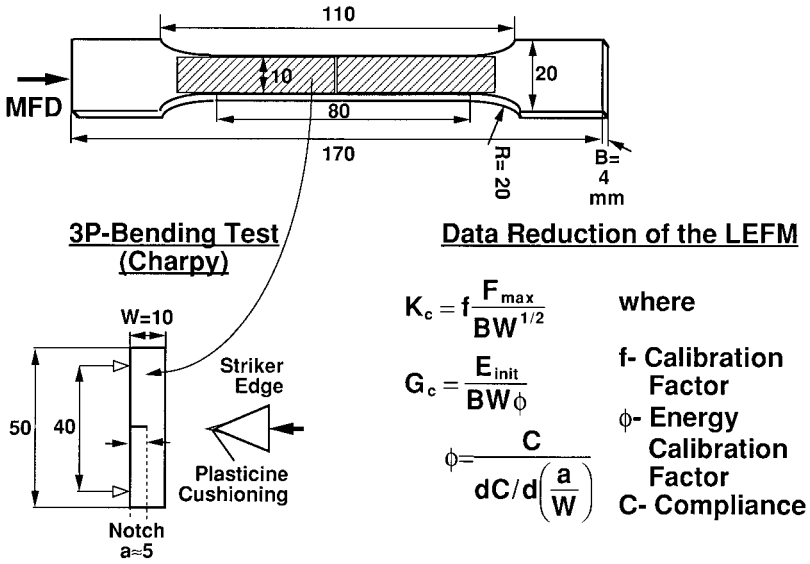

Figure 2 Machining, size (all data in mm), and loading of the notched Charpy bars cut from injection-molded dumbbells along with basic equations of the LEFM. Designation: MFD-mold filling direction.

The ductile failure manner can well be described by the ductility index (DI), the value of which is between 0 (fully brittle) and 1 (fully ductile failure):

$$\mathrm{DI} = \frac{E_{\mathrm{total}} - E_{\mathrm{init}}}{E_{\mathrm{total}}} = \frac{E_{\mathrm{prop}}}{E_{\mathrm{total}}} \qquad (1)$$

By contrast, the α-iPP fractured brittlely—the Charpy specimen broke instantaneously after $F_{\max}$ was reached [Fig. 3(a)]. It is necessary to draw the attention here to a further peculiarity in the fracture response: the F–t trace of α-iPP displays superimposed load oscillations which are missing in the fractogram of the β-iPP [Fig. 3(b)]. This is a hint of the high damping behavior of β-iPP reported by Jacoby et al.[14] The DMTA spectra in Figure 4 demonstrate, in fact, that $tg\,\delta$ values of β-iPP lay higher than the α-iPP, for practically the whole temperature range scanned.

Fractograms registered at RT indicate a slight change in the brittle fracture of α-iPP, viz. some crack propagation takes place resulting in higher DI value [see Fig. 5(a) and Table I]. The ductile fracture mode of β-iPP becomes even more pronounced at RT [Fig. 5(b)]. The rationale behind this feature is that RT agrees with that of the glass transition temperature (T_g, or β-relaxation) of iPP, and T_g is where brittle–ductile transition generally occurs.

Figure 5(b) also implies that the specimen of β-iPP did not fully break at RT. This is based not only on the aforementioned ductility increase at T_g, in which adiabatic crack tip heating may also

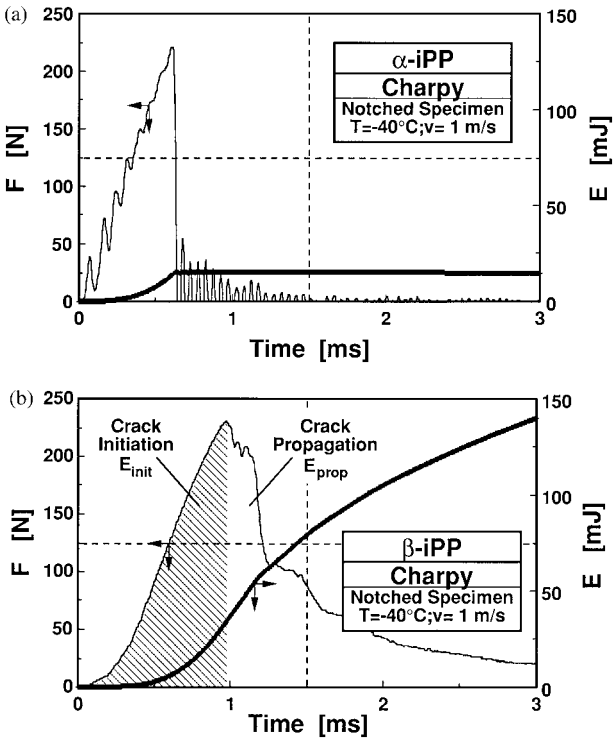

Figure 3 Comparison of the F–t and E–t traces of impacted notched Charpy specimens of (a) α-iPP and (b), β-iPP respectively, at $T = -40$°C.

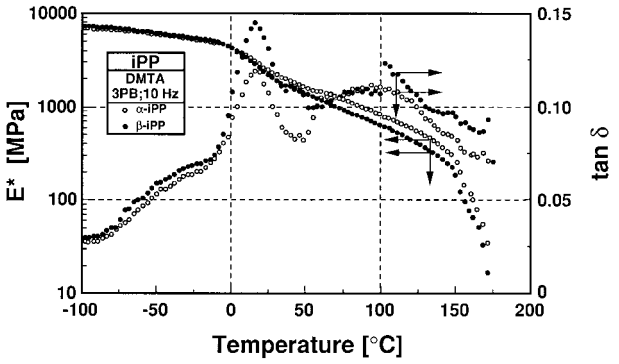

Figure 4 E^* and $tg\,\delta$ versus T traces for the α- and β-iPP, respectively.

be involved (see later), but also on the injection-molding-induced microstructure. Recall that the impact loading direction is perpendicular to that of the skin region, where the macromolecules and supermolecular structures are aligned in the MFD (see Fig. 2). This means an inherent (self) reinforcement,[24] the macroscopic appearance of which is the so-called plastic hinge, i.e., the impacted specimen is only partially broken (its halves are held together by this "hinge"). Therefore, neither E_{total} nor DI can be determined exactly (see Table I).

Figure 6 shows polarized light microscopic (PLM) pictures taken from the thickness section of the injection-molded α-iPP and β-iPP specimens and evidences the molding-induced skin-core structure. Figure 6 shows that the mean spherulite size in the core of β-iPP is smaller than the α-iPP, which means a higher ductility. Comparing the fractograms in Figure 5, one can state that the overall morphological effect of β-iPP is much higher than that of the α-iPP. It is noteworthy that the skin-(shear)-core structuring can be tailored by proper selection of the injection-molding parameters (e.g., mold temperature and injection speed).

Fracture Mechanical Response

Although the boundary conditions for application of the LEFM theory are strictly met only for the α-iPP at $T = -40$°C (ideally brittle fracture) and at RT (brittle fracture with some crack propagation), this approach also can be used for evaluation of parameters related to the fracture initiation even if the specimens break in ductile manner. The fracture mechanical data evaluated are listed in Table I.

Based on the fracture mechanical results in Table I, there is only a marginal difference in K_c between the α- and β-iPP. This is obviously due to the similar F_{max} values in the related fractograms (cf. Figs. 3 and 5). The fact that K_c increases with decreasing test temperature is in harmony with what is expected.

The basic difference in the impact fracture response is related to the initiation fracture energy (G_c) and DI. G_c of the β-iPP is ca. two times higher than the reference α-modification at both testing temperatures (cf. Table I). This toughness increment is considerably higher than that reported by Tjong et al. for injection-molded α- and β-iPP (G_c = 5.3 and 6.7 kJ/m^2, respectively).[16,17] It should be emphasized again that our α-iPP along with the specimen preparation technique are comparable with those of the cited authors, so that the difference in toughness can be attributed to effects of the β-nucleant and the higher molecular weight iPP used by us (extrusion grade in contrast to an injection molding grade studied by Tjong et al.)

Considering the fact that under plane stress conditions

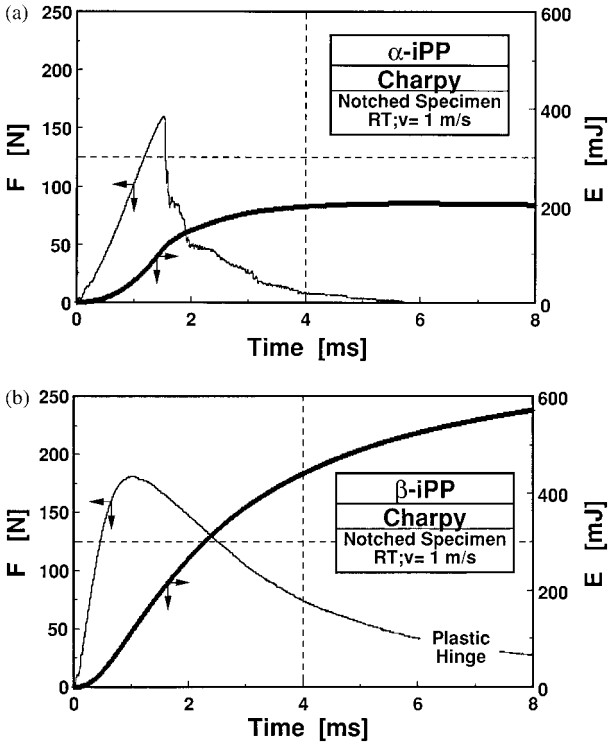

Figure 5 Comparison of the F–t and E–t traces of impacted notched Charpy specimens of (a) α-iPP and (b) β-iPP, respectively, at RT.

Table I Fracture Mechanical Data (K_c,G_C) and Ductility Index (DI) in High-Speed (v = 1 m/s) Three-Point Bending at T^2 = −40°C and RT for Injection-Molded α-iPP and β-iPP

iPP Form	K_c (MPa m$^{1/2}$)		G_c (kJ/m^2)		DI	
	−40°C	RT	−40°C	RT	−40°C	RT
α-iPP	4.0	3.3	5.4	8.5	0.04	0.3
β-iPP	4.3	3.9	8.5	19.8	≈0.40	>0.55

$$E = \frac{K_c^2}{G_c} \qquad (2)$$

holds, and the findings that K_c is about the same for both iPP forms, while G_c is higher for β-iPP, this implies that the E-modulus of the latter should be lower than the α-iPP. Based on the DMTA spectra in Figure 4 this is really the case, at least beyond T_g. At ambient temperature, E = 2.48 and 2.20 can be deduced for the α- and β-iPP, respectively, which is in agreement with literature data.[17] At T = −40°C the DMTA E-moduli of both versions are similar (E = 5.70 and 5.80 for α- and β-iPP, respectively). When the E-moduli are computed according to eq. (2) from the fracture mechanical data determined (cf. Table I), the results are markedly below the related values derived from DMTA measurements. What is the reason for this discrepancy? Since K_c data are by all means correct, the reason for this difference should rely on G_c. The fracture energy is substantially higher than expected for both iPP forms and especially for the β-iPP. There are several aspects which may responsible for the high fracture energy, such as morphological effects, crack tip blunting due to adiabatic heating, phase transformation, damping effects, and their combinations. Some of them work in both PP modifications (but in a different way), while the relative effects of others like $\beta\alpha$-phase transformation and mechanical damping (cf. Fig. 4) should turn out mostly for β-iPP.

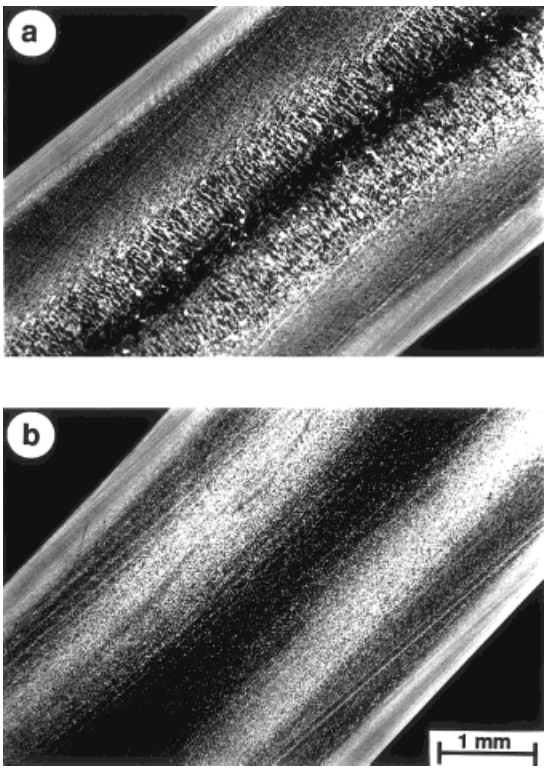

Figure 6 Polarized light microscopic pictures showing the injection-molding-induced skin–core structure in (a) α-iPP and (b) β-iPP, respectively.

It was shown earlier that ([25] and references therein) there is a correlation between fracture energy and $tg\,\delta$ in impact-toughened iPP irrespective of the difference in the testing frequency (based on Figs. 3 and 5, the test frequency during impact being ca. 10^3 Hz, whereas that of the DMTA was 10 Hz). Recall that $tg\,\delta$ of β-iPP is higher than that of α-iPP, especially beyond T_g (cf. Fig. 4), so damping may influence the fracture response. It should be underlined that the aforementioned toughness contributing terms are not independent of each other: for example, high mechanical damping is related to the morphology and the local morphology should affect the possibility of phase transformation as well. The fractographic work summarized below was therefore focused on these aspects.

Failure Mode

As mentioned in the introduction, the published SEM pictures taken from the fracture surface hardly reflect a two to three times improvement in

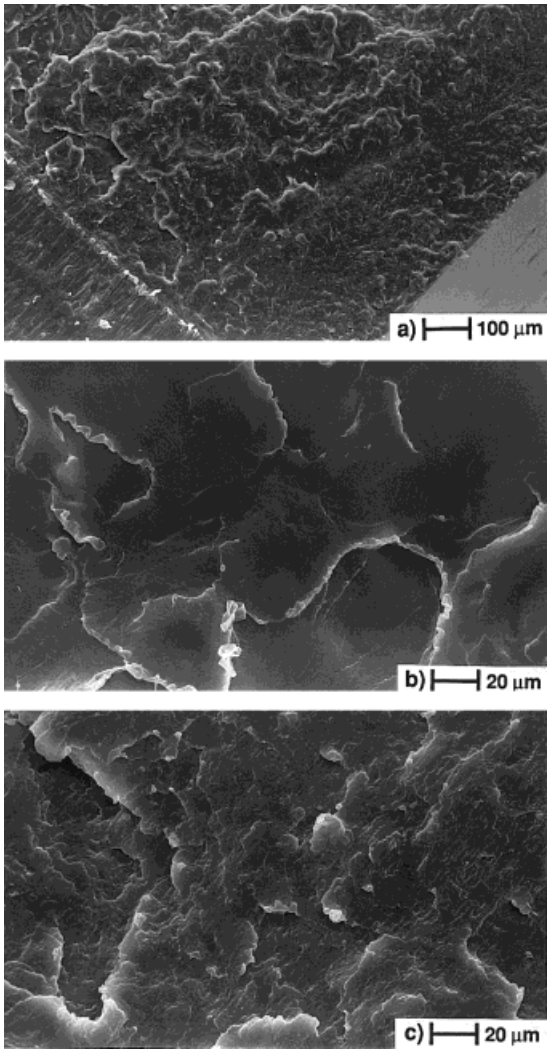

Figure 7 SEM microphotographs taken on the fracture surface of α-iPP broken at RT: (a) overall view, (b) core region, and (c) skin region. Notes: the boundary between the skin and core is indicated by arrow; (b) and (c) were taken from the vicinity of the razor notch.

toughness. Figure 7 displays the overall fracture surface [Fig. 7(a)] along with higher-magnification sections taken from the core [Fig. 7(b)] and skin [Fig. 7(c)], respectively, of a Charpy specimen of α-iPP failed at RT. The surface pattern in Figure 7(a) helps us to identify the skin thickness (ca. 0.4 mm). This is in accordance with the skin thickness deduced from the PLM picture in Fig. 6(a). Figure 7 indicates brittle fracture with some microductility, which is more perceptible at a closer view. The possible reason for the spots with microductile rims is coalescence of secondary cracks, which are generated beneath the main crack plane and affect mostly the crack propagation stage [cf. Fig. 5(a)].

Figure 8 shows SEM pictures taken from the fracture surface of a β-iPP specimen failed at RT. Figure 8(a) makes obvious that ductile failure is responsible for the enhanced fracture energy of β-iPP. Based on the ductile tearing pattern of the fracture surface, one can clearly see that the resistance to crack growth in the skin and core is markedly different. The skin thickness in β-iPP, estimated by the surface appearance, was ca. 0.4 mm, which agrees with PLM results [cf. Fig. 6(b)]. High-magnification SEM pictures taken from the notch vicinity in the core [Fig. 8(b)] and skin [Fig. 8(c)] contribute to a deeper understanding of the fracture mode. The porous structure just ahead of the notch is in close analogy to the stress-whitened zone found in static tests.[11–13] It was

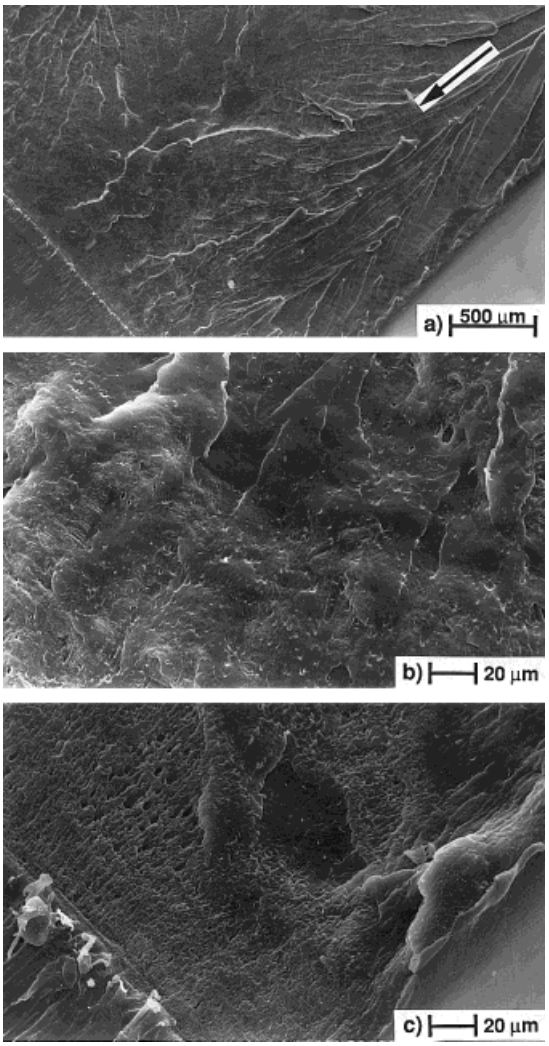

Figure 8 SEM microphotographs taken on the fracture surface of β-iPP broken at RT: (a) overall view, (b) core region, and (c) skin region.

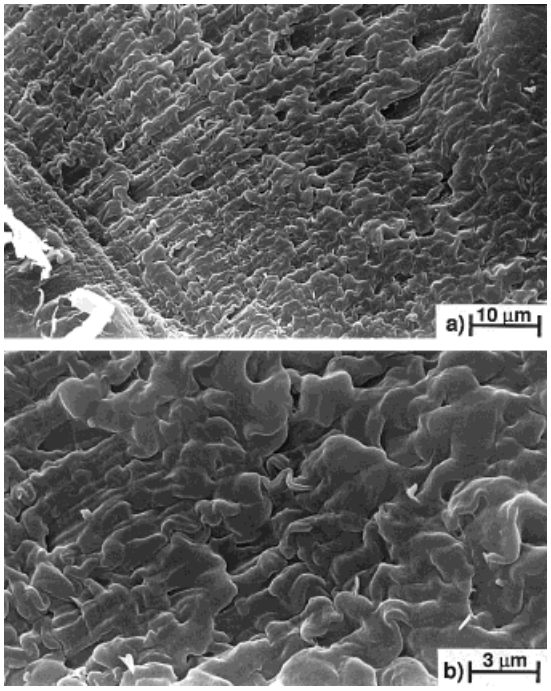

Figure 9 High-magnification SEM pictures taken from the fibrillated skin region.

shown that the plastic zone produced by static loading consists of microvoids, pores, that reflect the light and thus give rise of "stress-whitening." Their appearance was traced to phase transformation ($\beta\alpha$[11–13] and β-to-smectic[13]), accompanied with volume contraction. The latter was claimed to be dependent also on the local morphology.[13] Considering the fact that the relative occurrence of microvoids is higher in the skin than in the core [cf. Fig.7(b,c)], the aforementioned microstructural "constraint" effect may indeed contribute to the microvoid formation.

Figure 9 depicts high-magnification SEM pictures taken from the notch vicinity. Here remnants of microfibrils of a previously voided, crazed region can be observed. These microfibrils seem to be broken up under heat influence. The heat caused by high-speed impact bounce cannot be dissipated, and thus adiabatic crack tip heating may occur. That is the reason why the surface structure does not reflect the usual craze remnants (being "overwritten" by heat effects). Comparing the fracture surfaces in Figures 7 to 9, one can estimate that G_c of the β-iPP should lie markedly higher than α-iPP, at least at RT.

Unfortunately, we failed to demonstrate by the DSC technique that $\beta\alpha$-transformation took place and thus PPT would be responsible for the toughness enhancement. Phase transition may have occurred in a very thin layer so that bulk characteristics were measured by DSC. Indirect evidence for the $\beta\alpha$-transition is supplied, however, by Figures 8 and 9, where microvoiding and cavitation are clearly visible. There is a further but still indirect argument for the supposed $\beta\alpha$-transformation: It is known, that the skin layers stay under compression, while the core is under tensile stresses due to the solidification process in injection molding.[26] It can thus be argued that a transition with volume contraction should take place mostly in the skin. This was, indeed, found [see Figure 8(c)].

The above failure scenario is changed markedly by decreasing temperature. Figure 10 displays characteristic SEM pictures taken from the fracture surface of β-iPP broken at $T = -40$°C. The injection-molding-induced skin–core structure is quite perceptible again in Figure 10(a). The core fracture surface at high magnification is analogous to that of the α-iPP at RT [cf. Fig. 7(b)]. Considering the fact that the G_c value of α-iPP at RT is identical to that of β-iPP at $T = -40$°C (see Table I), the analogy in the related fracture surfaces is clear evidence of how predictable the fractography is. The main difference between the

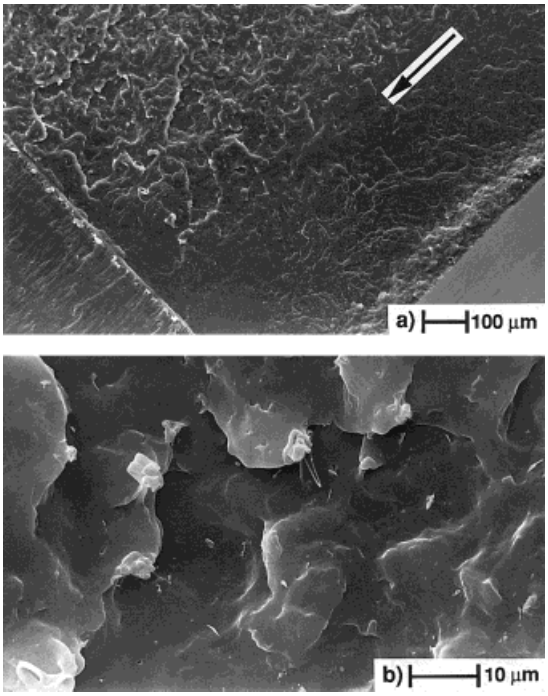

Figure 10 SEM microphotograph taken on the fracture surface of β-iPP broken at $T = -40$°C: (a) overall view and (b) core region.

failure of α-iPP at RT [Fig. 7(b)] and β-iPP at $T = -40$°C [Fig. 10(b)] is, however, that secondary cracking for the latter is more pronounced. Moreover, this secondary cracking is accompanied with some fibrillation (being, however, far less marked than at RT). It is worth noting that the fracture surface of the β-iPP specimen broken at RT, as published by Tjong et al.,[16,17] is very similar to what we got at $T = -40$°C. In addition, the related G_c values are comparable, as well (G_c = 6.7 and 8.5 kJ/m^2 according to Tjong et al. and this study, respectively).

Remnants of the individual fibrils in Figure 10(b) seem to reflect again some crack tip heating. The secondary cracking in β-iPP is likely to be affected (or even induced) by the β-nucleating salt particles. The dimplelike rough fracture surface [Fig. 10(b)] is therefore possibly a product of coalescence of secondary cracks that have been generated by the β-nucleating particles acting as stress concentrators. The above failure process is encouraged by the crystalline β-modification of iPP (including the related supermolecular formation) itself, which is more prone to both normal and shear-type deformation than the α-form.[27] The macroscopic appearance of this is that β-iPP has a lower yield strength than the α-iPP.[10] It should be mentioned here that smaller spherulite size of β-iPP (see Fig. 6) is a ductility increasing term, as well. Further investigations are needed, however, to clarify whether or not the "fibrillation" is linked to the density of tie molecules, as assumed.[16,17] Fujiyama demonstrated recently that the difference in the Izod impact strength between injection-molded (i.e., with skin–core structure) β- and α-iPP decreases, and even diminishes, with increasing MFI of the iPP resin.[28] Since increasing MFI is associated with a reduction in the mean molecular mass and thus with an analogous tendency in the density of the tie molecules, the finding of Fujiyama can be attributed to decreasing tie molecule density. Our results (based on an extrusion-grade iPP), compared to those of Tjong et al.,[16,17] achieved on an injection molding iPP, seem to corroborate this hypothesis as well.

CONCLUSIONS

The results of this study of the impact fracture and related failure behavior of injection-molded, notched α- and β-isotactic polypropylene (α- and β-iPP, respectively) fractured in high speed (v = 1 m/s) Charpy tests at $T = -40$°C and room temperature (RT), respectively, can be summarized as follows:

1. The fracture toughness (K_c) of α- and β-iPP differs only marginally in contrast to the fracture energy (G_c) values. G_c of the β-iPP was approximately double that of the reference α-iPP at both testing temperatures. Due to the microductile, ductile failure of β-iPP, it is recommended to adopt techniques of the postyield fracture mechanics instead of the linear elastic (LEFM) approach.
2. It was supposed that the superior toughness of β-iPP is a combined effect of the following: morphology (skin–core structure, crystal structure, spherulite size, tie molecules), mechanical damping, and phase transformation (β-to-α transition for which several indirect evidences are supplied). The relative contributions of the above terms change with the impact testing temperature.

This work was done for a research project supported by DFG (Ka 1202/4-1) and Volkswagen Foundations. The authors wish to thank Prof. G. Bodor (Technical University of Budapest, Hungary) and Mrs. A. Breining (University Erlangen, Germany) for the WAXS study and injection-molding of the specimens, respectively.

REFERENCES

1. J. Varga, in *Polypropylene: Structure, Blends and Composites,* J. Karger-Kocsis, Ed., Chapman & Hall, London, 1995, Vol. 1, Chap. 3.
2. J. Varga, *J. Thermal. Anal.,* **35,** 1891 (1989).
3. J. Varga, *J. Thermal. Anal.,* **31,** 165 (1986).
4. G. Shi, B. Huang, J. Zhang, and Y. Cao, *Scientia Sinica, Ser. B.,* **30,** 225 (1987).
5. F. J. Padden and H. D. Keith, *J. Appl. Phys.,* **30,** 1479 (1959).
6. T. Asano and Y. Fujiwara, *Polymer,* **19,** 99 (1978).
7. T. Asano, Y. Fujiwara, and T. Yoshida, *Polym. J.,* **11,** 383 (1979).
8. T. Yoshida, Y. Fujiwara, and T. Asano, *Polymer,* **24,** 925 (1983).
9. G. Shi, F. Chu, G. Zhou, and Z. Han, *Makromol. Chem.,* **190,** 907 (1989).
10. J. Karger-Kocsis, *Polym. Bull.,* **36,** 119 (1996).
11. J. Karger-Kocsis, *J. Polym. Eng. Sci.,* **36,** 203 (1996).
12. J. Karger-Kocsis and J. Varga, *J. Appl. Polym. Sci.,* **62,** 291 (1996).

13. F. Chu, T. Yamaoka, H. Ide, and Y. Kimura, *Polymer,* **35,** 3442 (1994).
14. P. Jacoby, B. H. Bersted, W. J. Kissel, and C. E. Smith, *J. Polym. Sci., B: Phys.,* **24,** 461 (1986).
15. M. Fujiyama, *Intern. Polym. Process.,* **10,** 172 (1995).
16. S. C. Tjong, J. S. Shen, and R. K. Y. Li, *Scripta Metallurg. Mater.,* **33,** 503 (1995).
17. S. C. Tjong, J. S. Shen, and R. K. Y. Li, *Polym. Eng. Sci.,* **36,** 100 (1996).
18. J. Varga, *J. Polym. Eng.,* **10,** 231 (1991).
19. B. Monasse and J. M. Haudin, *Colloid. Polym. Sci.,* **263,** 822 (1985).
20. J. Varga and J. Karger-Kocsis, *J. Polym. Sci. B: Phys.,* **34,** 657 (1996).
21. A. Turner-Jones, J. M. Aizlewood, and D. R. Beckett, *Makromol. Chem.,* **75,** 134 (1964).
22. A. Pavan, *High-Rate K_c & G_c Testing on Polymers,* testing protocol by the ESIS TC-4 ("Polymers and Composites") group, Milan, Italy, March, 1993.
23. E. Plati and J. G. Williams, *Polym. Eng. Sci.,* **15,** 470 (1975).
24. J. Karger-Kocsis and K. Friedrich, *Intern. J. Fatigue,* **11,** 161 (1989).
25. J. Karger-Kocsis and V. N. Kuleznev, *Polymer,* **23,** 699 (1982).
26. J. Kubát and M. Rigdahl, *Polymer,* **16,** 925 (1975).
27. M. Aboulfajar, C. G'Sell, B. Ulrich, and A. Dahoun, *Polymer,* **36,** 731 (1995).
28. M. Fujiyama, *Intern. Polym. Process.,* **10,** 251 (1995).